THE JOURNAL OF COMPARATIVE NEUROLOGY 464:1–16 (2003)

Retinal Remodeling Triggered by Photoreceptor Degenerations

BRYAN W. JONES,[1]* CARL B. WATT,[1] JEANNE M. FREDERICK,[1]
WOLFGANG BAEHR,[1] CHING-KANG CHEN,[1] EDWARD M. LEVINE,[1]
ANN H. MILAM,[2] MATTHEW M. LAVAIL,[3] AND ROBERT E. MARC[1]
[1]John A. Moran Eye Center, University of Utah School of Medicine,
Salt Lake City, Utah 84132
[2]Scheie Eye Institute, Department of Ophthalmology, University of Pennsylvania
School of Medicine, Philadelphia, Pennsylvania 19104
[3]Beckman Vision Center, University of California, San Francisco School of Medicine,
San Francisco, California 94143-0730

ABSTRACT

Many photoreceptor degenerations initially affect rods, secondarily leading to cone death. It has long been assumed that the surviving neural retina is largely resistant to this sensory deafferentation. New evidence from fast retinal degenerations reveals that subtle plasticities in neuronal form and connectivity emerge early in disease. By screening mature natural, transgenic, and knockout retinal degeneration models with computational molecular phenotyping, we have found an extended late phase of negative remodeling that radically changes retinal structure. Three major transformations emerge: 1) Müller cell hypertrophy and elaboration of a distal glial seal between retina and the choroid/retinal pigmented epithelium; 2) apparent neuronal migration along glial surfaces to ectopic sites; and 3) rewiring through evolution of complex neurite fascicles, new synaptic foci in the remnant inner nuclear layer, and new connections throughout the retina. Although some neurons die, survivors express molecular signatures characteristic of normal bipolar, amacrine, and ganglion cells. Remodeling in human and rodent retinas is independent of the initial molecular targets of retinal degenerations, including defects in the retinal pigmented epithelium, rhodopsin, or downstream phototransduction elements. Although remodeling may constrain therapeutic intervals for molecular, cellular, or bionic rescue, it suggests that the neural retina may be more plastic than previously believed. J. Comp. Neurol. 464:1–16, 2003.

Indexing terms: retinitis pigmentosa; animal models; molecular phenotyping; plasticity; remodeling; cell death; retina

Rod and cone photoreceptors of the sensory retina drive signal-processing circuitries of the neural retina. Most retinal degenerations such as retinitis pigmentosa (RP) affect the sensory retina, and the resultant loss of photoreceptor input constitutes deafferentation of the neural retina. RP is a family of inherited retinal degenerations involving more than 40 known genes, with many mutations in the rhodopsin gene (http://www.sph.uth.tmc.edu/RetNet). These disorders progress through night blindness and photopic vision impairment at different rates, advancing to severe and sometimes total vision loss. Primary rod cell death is often followed by secondary loss of cones, effecting a substantial and sometimes complete destruction of the sensory retina, and a complete deafferentation of the neural retina. As clinical rescue of rods or cones is not yet feasible, cell-based (Young et al., 2000; Coffey et al., 2002) and bionic (Humayun et al., 1996; Chow and Chow, 1997; Zrenner et al., 1998) therapies have been explored as methods to provide surrogate inputs to the surviving neural retina.

Grant sponsor: National Eye Institute; Grant number: EY01919 (M.M.L.); Grant number: EY02162 (M.M.L.); Grant number: EY06842 (M.M.L.); Grant number: EY08123 (W.B.); Grant number: EY02576 (R.E.M.); Grant sponsor: Research to Prevent Blindness (M.M.L., W.B., C.K.C., E.M.L., A.H.M.); Grant sponsor: the Foundation Fighting Blindness (M.M.L., W.B., E.M.L., A.H.M.); Grant sponsor: the Macula Vision Research Foundation (M.M.L., W.B.).

Robert E. Marc is a principal of Signature Immunologics Inc., manufacturer of the anti-hapten IgGs used in this research.

*Correspondence to: Bryan W. Jones, John A. Moran Eye Center, University of Utah School of Medicine, Salt Lake City, UT 84132. E-mail: bryan.jones@m.cc.utah.edu

Received 10 January 2003; Revised 24 February 2003; 27 March 2003

DOI 10.1002/cne.10703

Published online the week of July 28, 2003 in Wiley InterScience (www.interscience.wiley.com).

The presumed preservation of the neural retina in advanced RP and allied diseases is central to cellular and bionic rescue and is often asserted or assumed (Scarlatis, 2000; Zrenner, 2002), although such preservation is based on limited evidence from early stages in rodent models of retinal degeneration. However, the neural retina in human RP is highly remodeled (Li et al., 1995; Fariss et al., 2000) and severely depleted of neurons in areas devoid of cones. Anatomical surveys of the macula in human RP (Stone et al., 1992; Santos et al., 1997; Humayun et al., 1999) document variable ganglion cell loss, from mild to severe, but well-preserved regions of the neural retina invariably possess surviving sensory retina harboring cones. Conversely, regions of high cone loss express both neuronal loss and remodeling (Marc et al., 2001), suggesting that cone loss and subsequent neuronal loss are related.

Analyses of acquired (de Raad et al., 1996) and inherited (Fletcher and Kalloniatis, 1996) rodent degeneration models reveal subtle changes in cellular molecular phenotypes in the neural retina, some even preceding rod degeneration. Subtle remodeling of rod pathways emerges rapidly in the *rd1* mouse (Strettoi and Pignatelli, 2000; Strettoi et al., 2002), in which a phototransduction defect evokes death of rods by postnatal day (pnd) 21. Rod-driven bipolar cells and horizontal cell axon terminals retract their fine dendrites, and rod bipolar cell axon terminals assume immature synaptic structures. Defects extend to cone circuits: both cones (Fei, 2002) and cone horizontal cells (Strettoi et al., 2002) in the young *rd1* mouse sprout new neurites, whereas cone bipolar cells retract dendrites (Strettoi et al., 2003). During human rod degeneration, surviving rods and horizontal and amacrine cells similarly extend anomalous neurites throughout the retina (Li et al., 1995; Fariss et al., 2000). However, many human and rodent retinal degenerations progress slowly, and no consensus on the fate of the inner retina has emerged, as aged rodent retinal degeneration specimens are rare and studies rarely extend beyond pnd 90. Furthermore, standard histology and ad hoc immunocytochemistry, in which small sets of probes are employed, are ineffective tools for tracking the fates of the 55–60 classes of cells (Masland, 2001) in the mammalian retina.

To explore the impact of advanced stages of deafferentation on the neural retina, we screened all retinal cells in a library of 20 human and 86 aged natural, transgenic, and knockout rodent retinal degenerations using computational molecular phenotyping (Marc et al., 1995; Marc and Cameron, 2002; Marc and Jones, 2002) and overlay electron microscopy (Marc and Liu, 2000). Most animal sample ages were in the pnd 150–900 interval. Although samples of retinas from advanced rodent ages are rare, our findings are consistent across many different forms of retinal degeneration: massive neural and glial remodeling follows loss of the sensory retina in rodents, mimicking the progression of human RP. Sensory deafferentation consequent to photoreceptor degeneration can thus activate neuronal and glial plasticity in the mature mammalian retina, perhaps through activation of the same plasticity mechanisms underlying sensory experience-induced rewiring in young mouse retina (Tian and Copenhagen, 2001).

MATERIALS AND METHODS

Specimens

Human RP tissue was obtained from The Foundation Fighting Blindness Retina Donor Program. Institutional approval for use of human eyes was obtained from the University of Pennsylvania and followed the tenets of the Declaration of Helsinki.

Our 20 samples of advanced RP included 16 simplex, 1 X-linked, 1 autosomal dominant (ad) RP, and 2 Usher's syndrome. All were fixed in phosphate-buffered aldehydes (pH 7.4), including 0.5–2% glutaraldehyde with postmortem intervals of 0.5–6.5 hours, and stored in 2% paraformaldehyde in 0.1 M phosphate buffer at pH 7.4 (in 1988–2000) until they were resin-embedded in 2000. Eighty-six samples, mostly of advanced ages (pnd 150–900) from 13 rodent models of retinal degeneration, were analyzed. All animal experiments were conducted according to the ARVO Statement for the Use of Animals in Ophthalmic and Vision Research, with approval of the Institutional Animal Care Committee at the University of Utah.

Animal tissues were harvested after halothane or intraperitoneal barbiturate anesthesia, followed by perfusion with or enucleation and immersion in buffered 0.5–2.5% glutaraldehyde/1% paraformaldehyde. Some tissues were postfixed in 1% buffered osmium tetroxide pH 6.0, and all were resin-embedded over the years 1987–2002.

All were processed for computational molecular phenotyping and electron microscopy as previously described (Marc et al., 1995; Marc and Liu, 2000; Marc and Jones, 2002). Specific models included the transgenic S334ter rat expressing a truncated rhodopsin at Ser334 (Steinberg et al., 1996); the transgenic P23H rat model of autosomal dominant (ad) RP with an N-terminal rhodopsin H mutation at P23 (Steinberg et al., 1996; Machida et al., 2000); the natural RCS rat with a *mertk* defect impairing rod outer segment phagocytosis (LaVail et al., 1975; D'Cruz et al., 2000); the natural *rd1* mouse model of autosomal recessive (ar) RP with a pde6β nonsense mutation (Keeler, 1996; Pittler et al., 1993); the transgenic GHL mouse model of adRP, with a triple V20G, P23H, P27L rhodopsin mutation (Frederick et al., 2001); the transgenic TG9N mouse, expressing the N-terminal fragment of mouse RGS9 (Chen et al., 1993); the natural *nr* mouse, with a chromosome 8 defect causing Purkinje cell and rod degeneration (Landis, 1975; LaVail et al., 1993; Campbell and Hess, 1996); the natural *or* mouse model of human microphthalmia, with a null mutation in the *chx10* homeobox gene (Robb et al., 1978; Buirmeister et al., 1996); the *Chx10/p27^{Kip1}* mouse—*p27^{Kip1}* knockout rescue model of the *or* mouse (Green et al., 2003); the natural *Agtpbp1* (formerly *pcd*) mouse with Purkinje cell and slow rod degeneration (Mullen and LaVail, 1975; Blanks et al., 1982; LaVail et al., 1982; Fernandez-Gonzalez et al., 2002); the natural *rd2* (formerly *rds*) mouse with a partial dominant *prph2* defect and slow rod degeneration (van Nie et al., 1978); the rho$^{-/-}$ knockout mouse model of human RP (Humphries et al., 1997); and the transgenic rhoΔ CTA mouse with truncated rhodopsin at Ser334. Sample numbers are indicated in Table 1.

Computational molecular phenotyping

Computational molecular phenotyping transforms cell anatomical data into multidimensional molecular signatures that can be parsed by classification algorithms to classify all cells formally into the major neuronal types, subtypes, and, ultimately, natural classes (Marc and Cameron, 2002; Marc and Jones, 2002), providing quantitative visualization as tissue theme maps. Unlike other immunocytochemical strategies, computational molecular phenotyping classifies all cell space and tracks the fates of the

TABLE 1. Remodeling in Retinal Degenerations[1]

Species	HS	tRN	tRN	RN	MM	tMM	tMM	MM	MM	koMM	MM	MM	tMM	tMM
Gene defect	Mixed	*rho*	*rho*	*mertk*	*pde6β*	*rho*	*rgs9*	?	*chx10*	$p27^{Kip1}$	Agtpbp1	*prp2*	*rho*	*rho*
Model	RP	S334ter	P23H	RCS	*rd1*	GHL	TG9N	*nr*	*or*	$chx10^{2}$	*pcd*	rd2	$rho^{-/-}$	rhoΔCTA
Specimens	20	9	12	7	9	8	19	3	3	1	2	1	4	8
Onset	?	P340	P372	P270	P610	P555	P160	P300	<P0	<P63	P321	>P151	>P365	>P541
Neurons														
Cell death	+	+	+	+	+	+	+	o	+	+	o	o	o	o
Strictures	+	+	+	+	+	+	+	+	+	+	o	o	o	o
dGly ACs/mm	2	4	6	12	2	6	35	2	—[3]	5	o	o	o	o
Fascicles	+	+	+	+	+	+	+	+	+	+	o	o	o	o
Microneuromas	+	+	+	+	+	+	+	+	+	+	o	o	+	+
Glia														
Migration	+	+	+	+	+	+	+	+	+	+	o	o	o	o
Columns	+	+	+	+	+	+	+	+	+	+	+	o	o	o
Seals	+	+	+	+	+	+	+	+	o	o	+	+	+	+
Other														
VC invasion	?	+	+	+	+	+	+	+	+	o	o	o	o	o
RPE invasion	+	+	+	+	+	+	+	+	+	o	o	o	o	o

[1]+, present; o, absent; ?, undetermined; IPL, inner plexiform layer; dGly ACs, displaced glycinergic amacrine cells; t, transgenic; ko, knockout; HS, *Homo sapiens;* RN, *Rattus norvegicus*; MM, *Mus musculus*; RPE, retinal pigmented epithelium; VC, vascular cell.
[2]The $p27^{Kip1}$ ko rescues hypocellularity in *chx10* but also exhibits neuronal remodeling.
[3]Only isolated retinal patches survive in *chx10*.

major retinal cell types and subtypes across different models and species with constant performance. All samples were processed in resin matrices as single specimens or stacks (Marc, 1999) for thin sectioning at 250 nm into serial arrays. The arrays were surface-probed (Marc et al., 1995) with IgGs targeting L-alanine, L-aspartate, L-glutamate, L-glutamine, glutathione, glycine, taurine, γ-aminobutyric acid (GABA; Signature Immunologics, Salt Lake City, UT), captured as 8-bit high-resolution (243 nm/pixel) images (Marc and Jones, 2002), mosaicked, and registered (PCI Geomatica V8.2, PCI Geomatics, Richmond Hill, Ontario, Canada) into large image databases, ≈ 2 Gb/sample. Classifications using isodata clustering (Marc and Jones, 2002), theme map generation, and analysis were performed on raw data channels by PCI Geomatica and custom software written in IDL (Research Systems, Boulder, CO). Molecular signals are visualized as selected rgb maps encoding three molecular signals as red, green, and blue, respectively, e.g., γGE → rgb assigns γ-aminobutyric acid, glycine and L-glutamate to red, green, and blue color channels, respectively.

Detailed theme map generation first involved production of raw classification theme maps (Marc et al., 1995; Kalloniatis et al., 1996), which is equivalent to the spatial logical *and* of all the classified channels. Thus no single channel completely matches the raw theme map, and there is an error kerf surrounding classified structures (Marc et al., 1995). Refined theme maps were produced by assigning all cells and structures in a single channel (e.g., the toluidine blue channel) to their aligned classes in the theme map (Marc and Cameron, 2002; Marc and Jones, 2002). All theme maps displayed in this manuscript were refined. For display only, raw data channels were linearly contrast-stretched over a 30–220-pixel value range and sharpened with unsharp masking. Monochrome images were density mapped and rgb images were intensity mapped (Marc et al., 1995). All images were prepared in Adobe Photoshop V7.01 (Adobe Systems, San Jose, CA).

Electron microscopy and overlay microscopy

Conventional transmission electron microscopy was performed as previously described (Marc and Liu, 2000) on 90-nm lead-stained sections on single-hole grids. Sections serial to the section reserved for electron microscopy were processed for molecular phenotyping, and the optical rgb or theme maps were registered to the ultrastructure as described above. Both high- and low-magnification montages were captured as conventional electron micrographs and scanned as 8-bit monochrome channels at 300–600 dpi. Large databases were assembled from the ultrastructural images as described in Marc and Liu (2000) and then registered to scaled optical microscope data.

RESULTS

Computational molecular phenotyping of retinal degenerations

The objective of this work was to track the fates of all the major groups of retinal cells. Serial monochrome images of normal rat retina probed for different small molecules display patterns of labeling similar to those of other mammals (Fig. 1). No single probe captures all cells, but, taken together, virtually all cellular elements can be grouped into well-known classes or superclasses. The mapping of signals as γGE → rgb triplets permits visualization of large cohorts, such as GABA+ and glycine+ amacrine cells, photoreceptors, bipolar cells, and ganglion cells (Fig. 2A), whereas the mapping of τQE → rgb sets apart Müller cells, the retinal pigmented epithelium, and other elements from all other cells (Fig. 2B). The rat shows essentially the same composite patterns of small-molecule signatures as those in the primate, cat, and rabbit retinas (Fletcher and Kalloniatis, 1996; Kalloniatis et al., 1996; Marc et al., 1998; Marc, 1999). Classifying all the data with isodata clustering produces raw theme maps, which are then converted to refined theme maps (see Materials and Methods) superimposed on a single reference channel (Fig. 2C,D). Theme maps and rgb displays simplify tracking of 10 major cell phenotypes in retinal degeneration material: photoreceptors, horizontal cells, ON-center cone bipolar cells identified as glycine+ bipolar cells (e.g., Kalloniatis et al., 1996), all remaining bipolar cells as a mixed group of rod and OFF-center cone bipolar cells, glycine+ amacrine cells, GABA+ amacrine cells, ganglion cells, Müller cells, vascular elements, and the retinal pigmented epithelium. These 10 phenotypes account for virtually all retinal space.

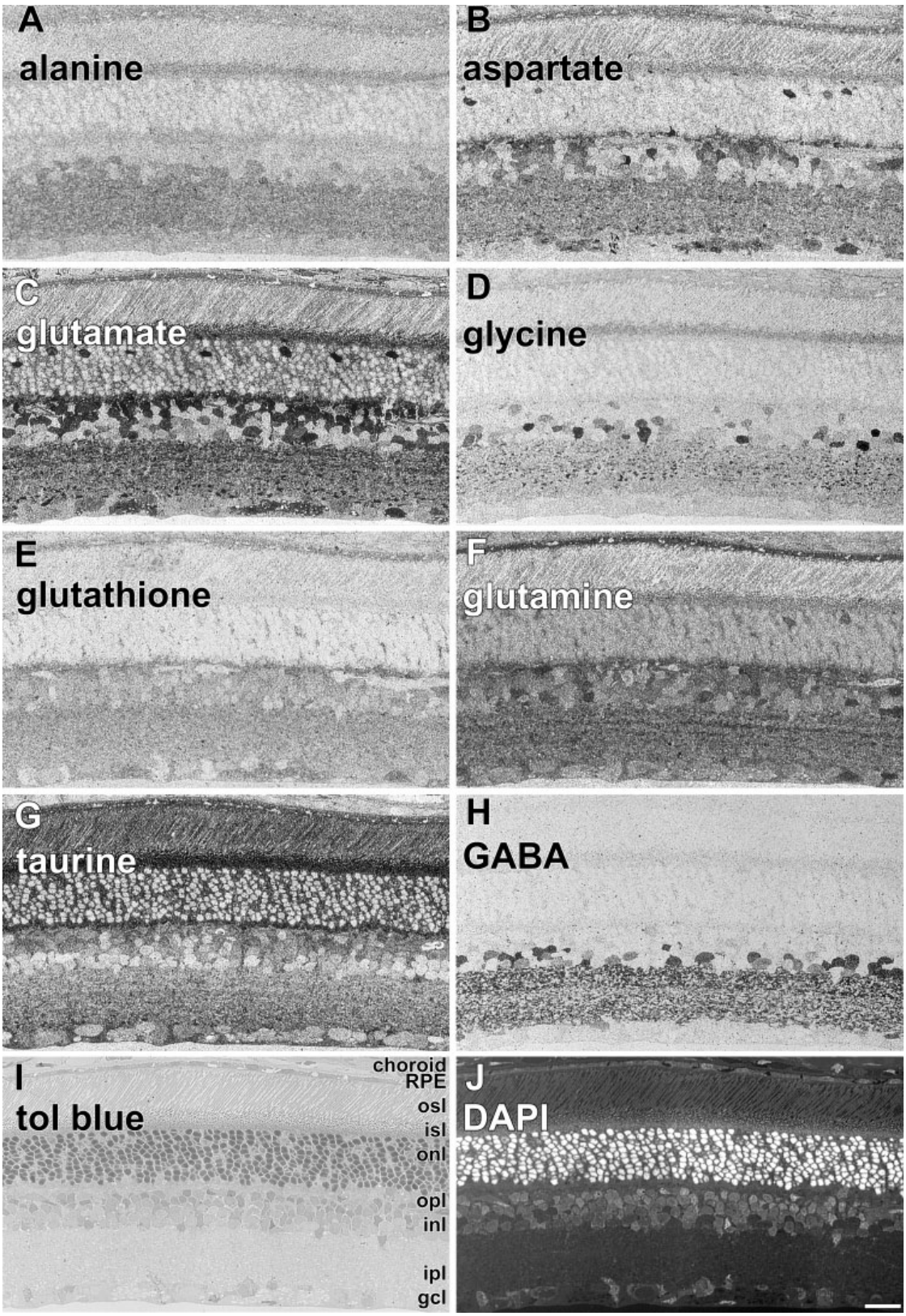

Fig. 1. Normal rat retina. Ten monochrome images from a series of 12,250-nm sections. Each section was also double-labeled with DAPI. **A:** alanine, section 1. **B:** Aspartate, section 2. **C:** Glutamate, section 9. **D:** Glycine, section 10. **E:** Glutathione, section 5. **F:** Glutamine, section 6. **G:** Taurine, section 7. **H:** GABA, section 11. **I:** Toluidine blue (tol blue), section 12. **J:** DAPI, section 11. Layers indicated in I: gcl, ganglion cell layer; inl, inner nuclear layer; ipl, inner plexiform layer; isl, inner segment layer; opl, outer plexiform layer; osl, outer segment layer; onl, outer nuclear layer; RPE, retinal pigmented epithelium. Scale bar = 20 μm.

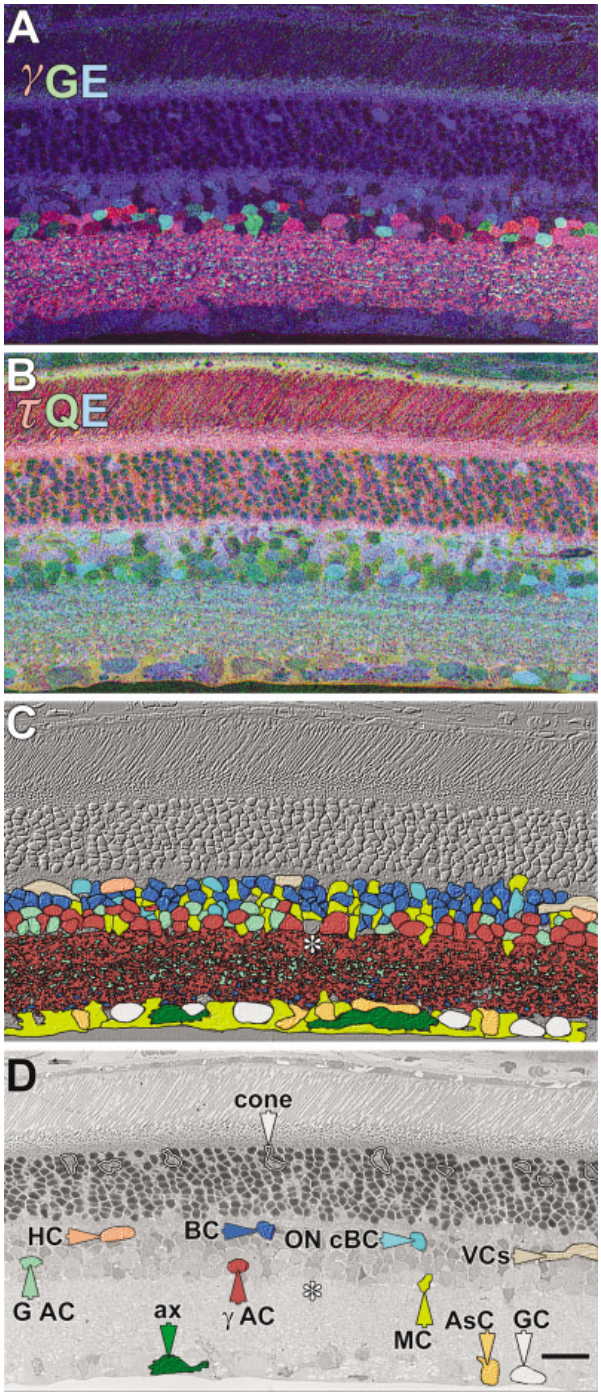

Fig. 2. Multichannel rgb mappings and theme maps from normal rat retina. **A:** γGE → rgb mapping. **B:** τQE → rgb mapping. **C:** Refined theme map superimposed on a monochrome digital phase version of the toluidine blue channel. **D:** The theme map key superimposed on raw toluidine blue monochrome channel. AsC, astrocyte; ax, axon bundle; BC, OFF-center cone and ON-center rod bipolar cell superclass; ON cBC, ON center cone bipolar cell; G AC, glycine+ amacrine cell; γ AC, GABA+ amacrine cell; GC, ganglion cell; HC, horizontal cell; MC, Müller cell; VC, vascular cells (endothelia + pericytes). Outlines, cone nuclei. Asterisk, unclassified cell. Scale bar = 20 μm.

Analysis of theme and rgb maps of 13 retinal degeneration models reveals that late remodeling does not appear until the outer nuclear layer is depleted of rods and cones and a seal of Müller cell processes is formed between the remnant retina and the choroid or any surviving retinal pigmented epithelium (Figs. 3, 4). Different initial defects in the various rodent models influence the timing and coherence of cell death in the sensory retina, resulting in different earliest onset times for remodeling of the neural retina (Table 1), spanning rapid (TG9N, P160) to slow onsets (RCS, P270) for models for which we have sufficient numbers of samples. Later onset times in Table 1 (e.g., *rd1*) reflect large gaps in our age samples between very young and old animals. As the study progressed, it became clear that it would be desirable to screen intermediate times, but that would require breeding new animals, requiring many years to produce complete chronologies. Despite uncertainty regarding precise onset times, two things are clear: as long as identifiable photoreceptors exist in the residual outer nuclear layer, remodeling is absent or cryptic; when remodeling is present, it exists in stereotyped form in most of retinal degenerations. Remodeling involves 10 major types of restructuring of the retina, as follows:

1. Neuronal death as evidenced by focal or global cell depletion, including instances of massive ganglion cell loss.
2. Relocation of all types of surviving neurons, including eversions of amacrine cell somata to the distal surface of the remnant retina and inversion of amacrine and bipolar cell somata to the ganglion cell layer.
3. Fragmentation of the inner plexiform layer lamination into frequent, small tracts of processes we term *strictures*.
4. Evolution of new neurites in complex fascicles surrounded by Müller cell processes.
5. Evolution of new foci of synaptic neuropil (microneuromas) in the remnant inner nuclear layer and formation of new synapses throughout the retina.
6. Migration of Müller cell somata to both distal and proximal borders of the retina.
7. Formation of hypertrophic columns of Müller cells.
8. Formation of a thick seal of Müller cell processes at the distal margin of the retina.
9. Invasion of blood vessels from both the vitreal and choroidal margins of the retina.
10. Invasion of retinal pigmented epithelium cells or apical processes deep into the retina.

Each of these events is a complex process, and this paper will be restricted to analysis of the neuronal and glial events in remodeling.

Figures 3 and 4 survey instances of remodeling in human and rodent retinal degenerations as γGE → rgb maps and theme maps. Taken together, most retinal degenerations display extensive remodeling, and the examples shown are unexceptional, culled from thousands of examples and more than 100 Gb of optical and electron microscopic image data. Due to space considerations, the companion τQE maps identifying Müller cells are not shown, but Müller cells and their processes are indicated on the rgb images of Figure 3 and the theme maps of Figure 4.

In advanced human RP, regions devoid of cones display massive remodeling, and the remnant tissue bears no resemblance to a normal retina. Evidence of neuronal migration is supported by the presence of glycinergic am-

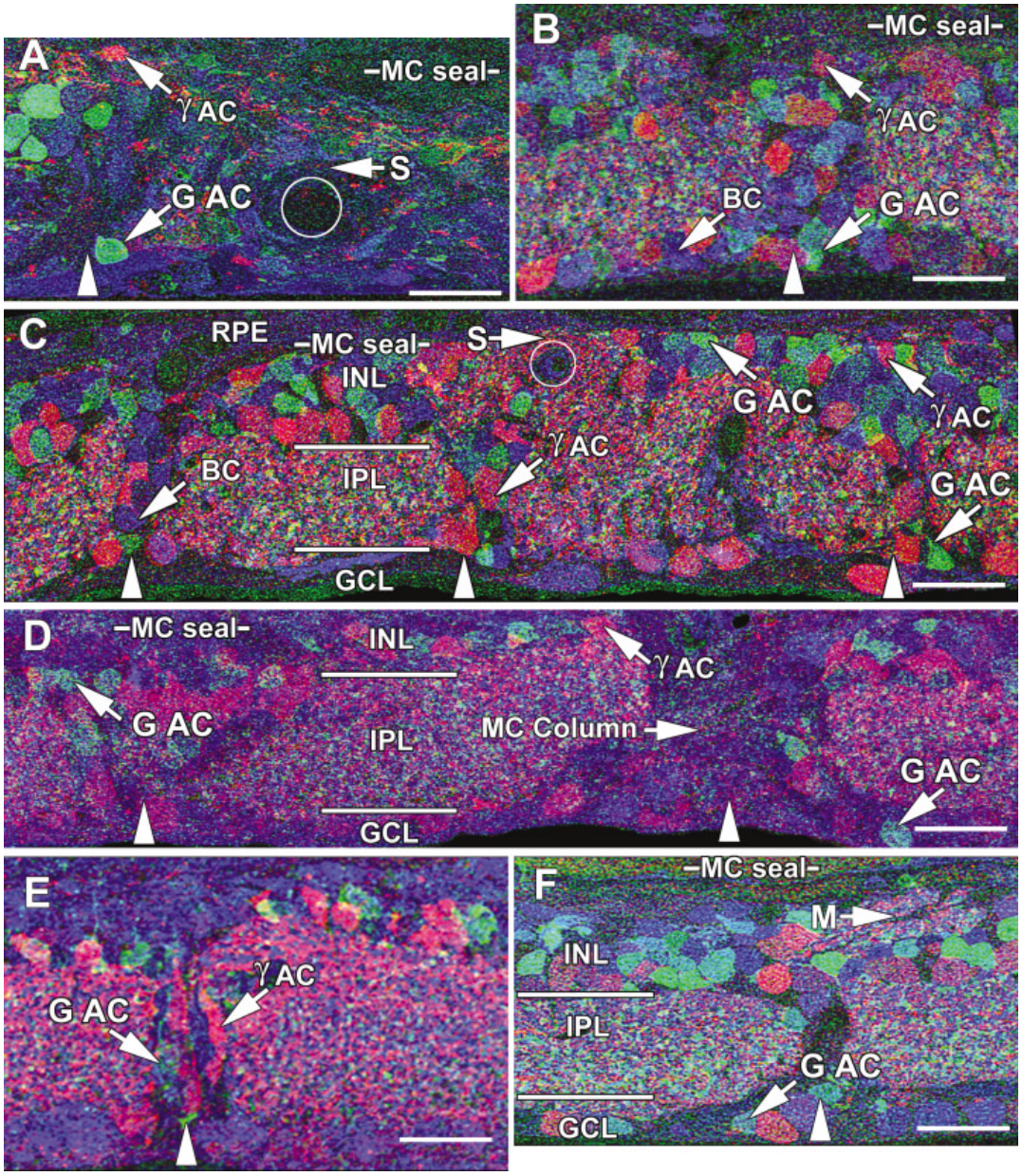

Fig. 3. Representative γGE → rgb mappings of retinal degeneration models. Downward arrows indicate inversions from the inner nuclear layer to the ganglion cell layer; upward arrows indicate eversions from the inner nuclear layer to the distal margin of the remnant retina; vertical arrowheads indicate glial columns; circles denote blood vessels. M, inner nuclear layer microneuroma; S, stricture; P, neuropil patch. All other abbreviations are as shown in Figures 1 and 2. **A:** Human RP retina, FFB accession #378, 76-year-old female, 2 hours post mortem, RP diagnosed at age 33, no vision at death. This vertical image demonstrates the massive cell loss typical of late-stage RP, with complete loss of the inner nuclear and ganglion cell layers at the right margin. A column of apparent neuronal migration is bordered by glycinergic amacrine cells in the ganglion cell layer and GABAergic amacrine cells at the distal margin of the remnant. Strictures distort the remaining inner plexiform layer, and a Müller cell fibrotic seal separates the retina from the choroid/retinal pigmented epithelium. **B:** *rd1* mouse, pnd 630. A large column of neurons bridges the depleted inner nuclear layer, displaying inverted amacrine and bipolar cells and everted amacrine cells. **C:** RCS rat retina, pnd 900. This image shows three columns of neuronal migration (vertical arrowheads) in which bipolar and amacrine cells are displaced from their proper locations. Distorted regions of the inner plexiform layer often pass through strictures as small as 5 μm. **D:** S334ter rat, pnd 363. This image shows two glial columns (vertical arrowheads), with right column exhibiting Müller cell hypertrophy breaking up the normal tiling of the retina. Everted and inverted glycinergic amacrine cells are abundant. **E:** P23H rat, pnd 372. A glial column (vertical arrowhead) traverses the inner plexiform layer accompanied by migrating glycinergic and GABAergic amacrine cells. **F:** GHL mouse, pnd 746. A broad glial column (vertical arrowhead) serves as a pathway for migration for amacrine and bipolar cells into the ganglion cell layer. A microneuroma has formed distal to the heavily depleted inner nuclear layer.

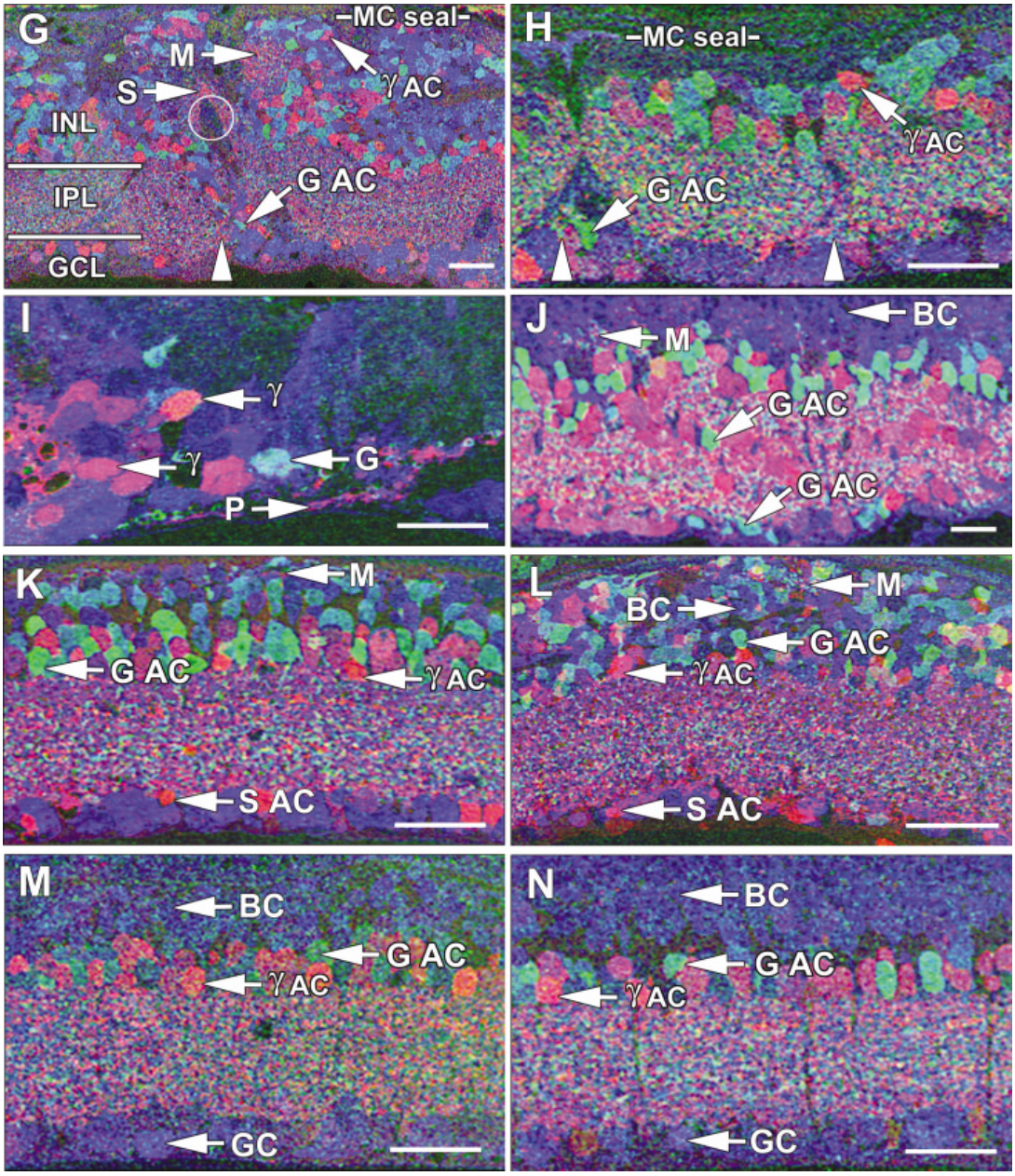

Fig. 3. (Continued). **G:** TG9N mouse, pnd 160. An oblique column forms a neuron migration path with both inverted and everted cells. Strictures deform the inner plexiform layer, and microneuromas form in the midst of the inner nuclear layer, but a mere 5 μm from the distal glial seal. **H:** *nr* mouse, pnd 720. Two columns of neuronal migration are indicated, with inversion and eversion of amacrine cells. The inner nuclear layer is thinned to less than half its normal thickness. **I:** *chx10* mouse, pnd 365. Few neurons survive in this defect, and only in small clusters with tiny patches of apparent neuropil surrounded by massive fields of apparent Müller cells. **J:** *Chx10/P27*$^{Kip1-/-}$ hypocellularity rescue mouse, pnd 60. This model initially displays roughly normal lamination, but with few bipolar cells and severely reduced photoreceptor numbers. However, even in the absence of clear glial columns or seals, microneuromas emerge, and columns of neurons strung through the inner plexiform layer are common, as are misplaced amacrine cells in the ganglion cell layer. **K:** RKO mouse, pnd 365. No neuron migration has emerged, and positions of amacrine cells, including presumed starburst amacrine cells (S AC), are normal. However, microneuromas are forming next to the glial seal. **L:** RhoΔCTA mouse, pnd 541. Migration across the inner plexiform layer has not begun, but microneuromas are emerging and the entire inner nuclear layer displays disordering of neurons, with everted amacrine cells and bipolar cells moving into the former amacrine cell layer. **M: pcd** mouse, pnd 321. At this age, retinal lamination appears normal and no microneuromas have emerged. **N:** *rd2* mouse, pnd 151. At this age, retinal lamination appears normal and no microneuromas have emerged. These image data will be available for public access at http://prometheus.med.utah.edu/~marclab/. Scale bar = 20 μm.

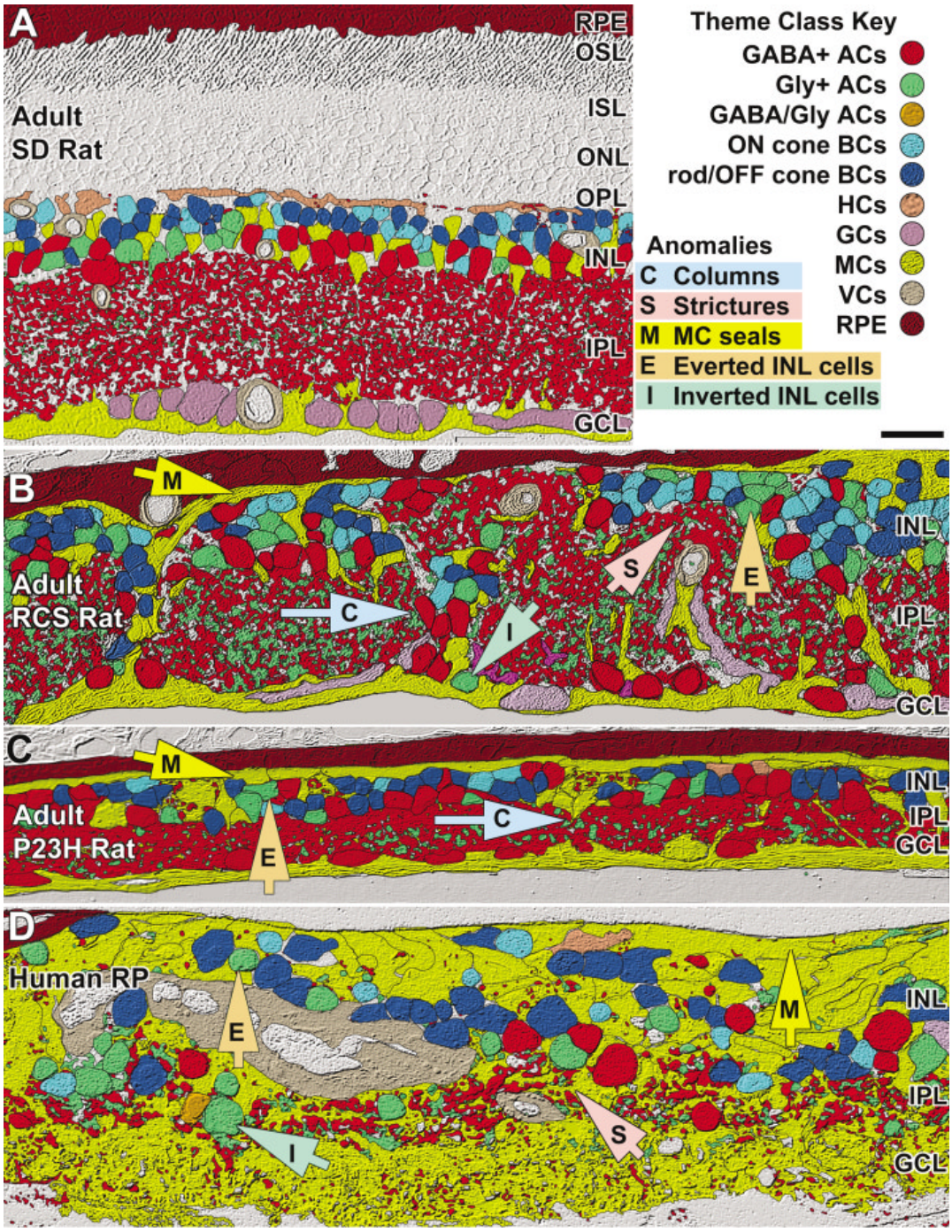

Fig. 4. Theme maps of (**A**) normal pnd 700 Sprague-Dawley (SD) rat, (**B**) pnd 900 RCS rat, (**C**) P372 P23H line 1 transgenic rat, and (**D**) human RP (Foundation Fighting Blindness accession #133-OD, 67-year-old female, advanced RP, simplex, fixed 2.5 hours post mortem). In normal retina, cell layers are precisely defined. Remodeling clearly disrupts lamination via migration on Müller glia columns (C), yielding eversion (E) of GABAergic and glycinergic amacrine cells to the distal Müller glial seal (M) and inversion of amacrine and bipolar cells (I) to the ganglion cell layer. Glial hypertrophy and neuronal movement can be so extensive that the inner plexiform layer is segmented, distorted. and forced through strictures (S) as small as 10 μm. Abbreviations as in Figures 1 and 2.

acrine cells at the proximal margin of the retina, nominally the remnant ganglion cell layer, and by GABAergic amacrine cells at the distal margin of the retina (Fig. 3A). Using the inversion of glycinergic amacrine cell somata to the ganglion cell layer as a semiquantitative index of remodeling, we determined the incidence of misplaced glycinergic amacrine cells in the normal mammalian retina (human, monkey, cat, rabbit, rat, mouse) in a linear aggregate of mammalian samples totaling over 1 meter (>500 individual glycine-probed sections ranging from 0.5 to 2 mm long). The probability of encountering a misplaced glycinergic amacrine cell in a vertical section is < 0.001/mm. The incidence of misplaced glycinergic amacrine cells in human, rat, and mouse retinal degeneration tissue ranges from 2 to 35/mm (Table 1) representing a 10^3–10^4 fold increase over misplaced glycinergic amacrine cells in the normal retina. In human and many rodent models, patches of retina completely devoid of neuronal somata in the inner nuclear or ganglion cell layers, or both, can also be located. These are so frequent that they cannot be due simply to depopulation by migration, and we interpret them as evidence of focal neuronal death. For example, a case of advanced human RP viewed as a theme map of all cellular space displays a complete absence of ganglion cells, virtually complete scrambling of the inner nuclear layer, and depletion of inner plexiform layer processes, accompanied by extensive Müller cell hypertrophy (e.g., Fig. 4D).

Of the rodent models examined, the natural *pde6*β nonsense mutation in the *rd1* model is an aggressive defect that rapidly kills rods, with eventual degeneration of the entire outer nuclear layer. By pnd 630, large columns of cells traverse the inner plexiform layer, with inversions of all types of amacrine and bipolar cells into the ganglion cell layer (Fig. 3B). We do not know the precise onset of remodeling in the *rd1* model.

Another transduction pathway defect model, the TG9N mouse, is a very aggressive degeneration that starts neural remodeling by pnd 160, with large tracts of neurons traversing the inner plexiform layer, numerous inversions of amacrine cells and bipolar cells to the ganglion cell layer, and eversions of amacrine cells to the distal seal (Fig. 3G). Disruptions of the inner plexiform layer lead to numerous neuropil strictures.

Defects in RPE function and rhodopsin expression generally lead to slower rod degenerations and later onsets of remodeling, but the outcomes are the same as the faster models. The RCS rat begins remodeling by pnd 270 and eventually displays massive reorganization of the inner nuclear and ganglion cell layers, with numerous hypertrophic columns of Müller cells surrounded by displaced neurons and disrupted inner plexiform layer segments (Figs. 3C, 4B). Very few identifiable normal ganglion cells remain in these regions, and most of the ganglion cell layer appears to be repopulated by new cells. Axon tracts become captured by the inward movement of vitreal vessels (Villegas-Perez et al., 1998), which also leads to the compression or displacement of neuropil, forming strictures (Fig. 4B). The theme map of glial processes in the RCS rat also shows the characteristic thick fibrotic layer that seals the neural retina from the choroid or any remaining retinal pigmented epithelium. This seal is often incomplete in advanced remodeling, and the remnant inner plexiform layer often approaches the distal limit of the retina at these breaks (Fig. 4B). This highly disordered neural retina can clearly be seen to bear little resemblance to a theme map of the normal rat retina.

In a transgenic model of rhodopsin truncation, we have examined advanced age samples (pnd 340–418) of four lines of the S334ter rat, which display different rates of rod degeneration, probably due to different transgene integration sites or integration of different transgene copy number. All lines show remodeling ranging from inner plexiform layer thinning and mild cell loss to severe restructuring, as shown in Figure 3D (pnd 363). As is common in almost all remodeling retinas, the inner nuclear layer is often reduced to a single layer of amacrine cells at the distal margin of the retina, whereas columns of amacrine cell and bipolar cells reposition into the ganglion cell layer. The depletion of the ganglion cell layer is difficult to gauge in the absence of whole mounts, for which aged animals would have to be raised, especially in the presence of amacrine cell migration from the inner nuclear layer, but long tracts of the ganglion cell layer spanning several hundred microns are depleted of cells.

We examined three lines of the P23H transgenic rat, a model for the most common form of human adRP. All show some remodeling, but again the severity varies. Over the pnd 372–410 interval, glial columns emerge, and with them the migration of inner nuclear layer neurons into the ganglion cell layer begins (Fig. 3E). Line 1 of the P23H transgenic rat is particularly aggressive and displays extensive neuronal cell death throughout the retina, depleting in excess of 90% of the retinal ganglion cells, thinning the amacrine cell layer to <10 μm in many regions, and often reducing the inner nuclear layer to a single layer of amacrine and bipolar cells (Fig. 4C).

The GHL transgenic model is the murine homologue of human adRP, the first system in which late remodeling was found (Jones et al., 1999) and the original impetus for this survey. The GHL mouse displays slow rod and cone loss in the first year of life (Frederick et al., 2001), but no major remodeling occurs in this phase, although rod circuitry may be altered in early degeneration stages, as in the *rd1* mouse (Strettoi and Pignatelli, 2000; Strettoi et al., 2002). An unknown mechanism eventually leads to cone death in this and other models (e.g., Mohand-Said et al., 1998; Fintz et al., 2003), and remodeling of the neural retina begins prior to pnd 555–746, by which time the GHL mouse retina displays many migrating neuronal columns, hypertrophic Müller cells, microneuromas, and glial seals (Fig. 3F). We do not have a precise onset of chronology for this model.

The rhoΔCTA model is the murine homologue of the S334ter rat and, although it displays rapid loss of rod photoreceptors, it does not remodel as quickly as the rat systems. By pnd 541, major glial columns have yet to emerge, but the distal seal is complete and microneuromas are forming in the distal retina (Fig. 3L). Despite a lack of migration through the inner plexiform layer, the inner nuclear layer is clearly disordered in the aged rhoΔCTA mouse, with Müller and amacrine cell somata repositioned at the distal margin of the retina and many bipolar cells in the amacrine cell layer.

The rhodopsin gene knockout mouse (RKO) also has a fairly gentle remodeling retina, as the initial waves of cell death seem highly rod-restricted. Eventually the entire outer nuclear layer appears ablated, and, similar to the rhoΔCT A model, microneuromas and inner nuclear layer cell migration occur (Fig. 3K). By at least pnd 365, however, no migration into the ganglion cell layer has

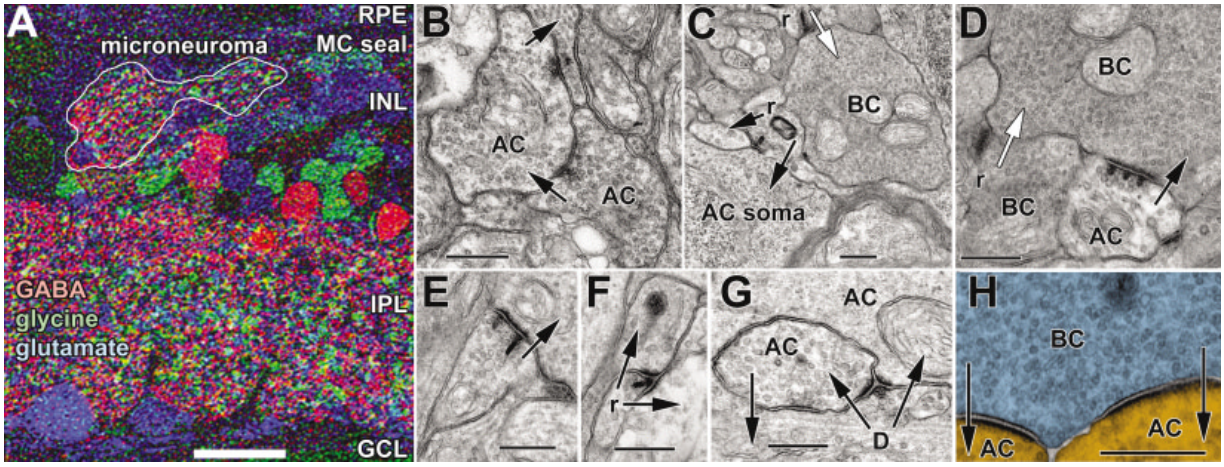

Fig. 5. Microneuromas and apparent retinal rewiring. **A:** γGE → rgb mapping of RCS rat retina showing the emergence of new neuropil beneath the distal Müller cell (MC) seal. Microneuromas are tangles of GABAergic (red), glycinergic (green), and glutamate+ (blue) neurites. **B:** Microneuroma amacrine → amacrine → target synapse chains. **C:** Anomalous bipolar → amacrine cell soma and bipolar → bipolar synapses. **D:** Presynaptic multiprojection amacrine → bipolar and bipolar → bipolar cell contacts. **E:** Multi-ribbon synapses. **F:** Classic bipolar cell presynaptic dyad element in a process ≈ 100 nm diameter, with few vesicles. **G:** Anomalous dyad-like synapse (D) with amacrine cell feedback. The presynaptic element contains few vesicles and resembles an amacrine cell dendrite. **H:** Theme map of a large bipolar cell terminal lacking ribbons but making large conventional contacts onto amacrine cell dendrites. The blue overlay denotes the signature of an ON-center cone bipolar cell; orange denotes GABAergic amacrine cells. Synaptic directions are indicated by arrows; white arrows, bipolar → bipolar cell contacts; r indicates synaptic ribbons. Scale bars = 20 μm in A; 200 nm in B–H.

emerged. Given the slowness of the remodeling in the GHL model, we might expect the RKO to show more complete remodeling by pnd 500.

Two Purkinje cell degeneration mutants are well known for inducing slow photoreceptor degenerations, although the mechanisms remain unclear. The *nervous* (*nr*) mutant expresses Müller cell seals and columns, neuronal inversion and eversion events, microneuromas, and significant neuron depletion in the inner nuclear layer (Fig. 3H). Remodeling is absent at 1 year, well under way by pnd 450, and extensive by pnd 730. Our oldest *pcd* sample (pnd 321) shows no evidence of remodeling, although the Müller cell seal is complete (Fig. 3M). If it progresses at the same rate as the *nr* mouse, we would not expect to see remodeling at this stage.

As in our pcd murine model, our oldest sample of the *rd2* mouse (formerly the *rds*, *rd slow* model) is still rather young by remodeling standards (pnd 151) and still possesses remnant cones and some rod nuclei (Fig. 3N). It displays no remodeling in the neural retina, and we would expect that, given the availability of older models, we would begin to see the same sequelae of retinal degeneration observed in other models.

The *or* hypocellularity mutant is a developmental defect caused by a natural *chx10* transcription factor gene null mutation. Although it is not a true post-maturation photoreceptor degeneration model, being a defect caused by impaired production of inner nuclear layer neurons, especially bipolar cells (Liu et al., 1994), the sequelae of the *or* defect far exceed simple loss of inner nuclear layer neurons. By pnd 365, there are no photoreceptors and no identifiable lamination, and virtually all of the retina is absent, except for tiny patches of roughly a dozen neurons accompanied by tiny foci of apparent neuropil (Fig. 3I). Although this may not represent the same kind of remodeling observed in retinal degenerations, it suggests that maintenance of a normal retinal structure may require a nearly complete cohort of neurons. The *chx10/p27^{Kip1}* double null mutation represents a quantitative but not qualitative proliferation rescue from hypocellularity, resulting in an abundance of amacrine cells, a reduced number of photoreceptors, and partially normal retinal lamination (Green et al., 2003). GABAergic and glycinergic amacrine cells are found in bands throughout the inner plexiform layer, misplaced to the ganglion cell layer, adjacent to the thinned outer nuclear layer, and engaged in microneuroma formation (Fig. 3J). However, the *chx10/p27^{Kip1}* double null mouse expresses neither a distal glial seal nor hypertrophic Müller cell columns.

Rewiring, microneuromas, and neurite fascicles

Remodeling neurons make new connections. Ectopic fascicles of hundreds of small neurites traverse the disordered inner nuclear layer along glial surfaces, elaborating 20–100-μm-diameter microneuromas at densities exceeding ≈ 30,000/retina in some models (GHL, TG9N, RCS). Microneuromas are tangles of GABAergic and glycinergic amacrine cell and glutamate+ cell processes (Fig. 5A), some extending additional tracts of neurites along glial seals and others merging with the remaining inner plexiform layer. New synapses are formed within these new sites in the remnant inner nuclear layer and around the somata of survivor neurons. Microneuromas contain both conventional and ribbon synapses and display abundant common synaptic arrangements: amacrine → amacrine (Fig. 5B), bipolar → amacrine (Fig. 5C), and amacrine → bipolar (Fig. 5D). The amacrine → bipolar contact of Figure 5D also bears a resemblance to multiprojection synapses of the cortex. Unusual bipolar → bipolar contacts are present in both microneuromas and the remnant inner plexiform layer (e.g., Fig. 5C,D), and various synapses are

made by and onto neuronal somata in the fragmented inner nuclear layer (e.g., Fig. 5C). Multi-ribbon and extremely small ribbon contacts are abundant (Fig. 5E,F), but we have also found these to be common in the normal rat retina. Complex contacts, such as amacrine cell feedback arrangements (Fig. 5G), are common but not detectably more so than in normal retina.

Finally, we have used multichannel overlay microscopy (Marc and Liu, 2000) to identify characteristic synaptic profiles as definitively bipolar or GABAergic amacrine cell elements (Fig. 5H). Unlike normal bipolar cells, this process in the remnant inner plexiform layer appeared to make large ribbon-free conventional, flat contacts onto target GABAergic amacrine cells. Although many forms of contacts in the inner plexiform layer proper appeared quite normal, including gap junctions between ON-center cone bipolar cells and glycinergic amacrine cells, we cannot determine whether most synaptic contacts in microneuromas represent proper or improper assemblies. The exceptions are bipolar → bipolar contacts, which do not occur in normal retina, new contacts associated with migrating neurons, ribbon contacts made by bipolar cell somata, and ribbon synapses onto the distal or lateral aspects of amacrine cells.

Overlay microscopy permitted us to determine the nature of some of the connections made by migrating neurons in remodeling retinas. Figure 6A is the ultrastructural channel (a montage) from a 6-channel registered dataset (GABA, glycine, glutamate, glutamine, taurine, ultrastructure) and shows a cluster of neuronal somata separated from the vitreous by a thin border of Müller cell processes and overlain by an irregular strip of remnant inner plexiform layer. The $\gamma G\tau \rightarrow$ rgb mapping (Fig. 6B) reveals that most of the cells are glycinergic amacrine cells that have migrated into the former ganglion cell layer. By using the rgb image as a transparent overlay, a complete map of cell identities is realized (Fig. 6D), including a glycinergic cell in the midst of the remnant inner plexiform layer and two classes of bipolar cell terminals: glycine+ (ON-center cone bipolar cells) and glycine- (either rod or OFF-center cone bipolar cells). At higher resolution, a small GABAergic terminal can be seen to make focal presynaptic specializations on the proximal aspect of the repositioned glycinergic amacrine cell. This probably represents formation of a new contact by GABAergic amacrine cell processes invading the ganglion cell layer.

Neurite fascicles are common within and distal to the remnant inner nuclear layer in remodeling retinas and are often visualized as bands of parallel processes or small punctae bearing characteristic inner plexiform layer signatures. At the optical level it is difficult to distinguish cross-sectioned neurite fascicles from small microneuromas, but overlay electron microscopy clearly reveals their nature and composition. Serial section channels of the distal RCS rat retina were probed for GABA, glycine, glutamine, taurine, and glutamate in addition to ultrastructure. The five-dimensional signatures from this signature dataset can be used uniquely to classify structures into ganglion, GABAergic amacrine, glycinergic amacrine, bipolar, and Müller cell profiles in all species (Marc et al., 1995; Kalloniatis et al., 1996). The aligned channels and theme maps may then be used to classify ultrastructural data at resolutions often exceeding the Rayleigh limit and with far superior signal-to-noise ratios than immunogold methods (see appendix in Marc and Liu, 2000). Figure 7A displays an ultrastructural theme map of a neurite positioned ≈ 2 μm proximal to the remnant retinal pigmented epithelium, and Figure 7B is the underlying monochrome image. The fascicle contains clear accumulations of ganglion, GABAergic amacrine, glycinergic amacrine, and bipolar cell-like processes, apparently segmented into preferential groups. The large ganglion cell dendrites (blue) tend to run together, as do the smaller GABAergic amacrine cell processes (red). The entire fascicle is encased and partially invaded by Müller cell processes. Similar structures were observed by ultrastructural analysis in GHL mouse retinas and by optical microscopy in S334ter rat, P23H rat, TG9N mouse, and *rd1* mouse retinas.

DISCUSSION

After loss of the outer nuclear layer, retinal remodeling ensues, leading to substantial topological, cell population, and connectivity changes. These include the emergence of a distal glial seal, inversions of amacrine and bipolar cell somata to the ganglion cell layer, eversions of amacrine cells to the distal margin of the retina, neuronal death, and extensive rewiring. The rodent neural retina clearly remodels in the same manner as human RP retinas. No normal vertebrate retina in our archive of more than 6,000 specimens and 40 species, including human retinas older than 65 years and rodent retinas of pnd 700 and greater, ever display any of these features of remodeling. Remodeling is not associated with senescence and is uniquely the sequel of disease. Remarkably, however, the basic signatures of retinal cells in advanced retinal degenerations are essentially indistinguishable from those of normal retinas. In some instances, glutamate levels are slightly elevated in Müller cells. In no cases do intermediate signatures emerge, and this suggests that remodeling phenomena do not trigger significant changes in the gene expression profiles that create the molecular phenotypes of the retina. This then allows us to track anatomical changes underlying remodeling with good cellular precision. Virtually all retinal degenerations display remodeling regardless of whether they are triggered by RPE failure, defects in rhodopsin expression, defects in transduction pathway elements, alterations in retinal progenitor cell proliferation patterns, or other mechanisms. Some genetic defects elicit little or no late remodeling (*rd2*, rho$^{-/-}$, *pcd*, or RhoΔCTA), as remnant cones persist for hundreds of days beneath the glial seal, albeit transformed in structure. However, given enough time, remodeling may emerge, as patches of cone loss in the *pcd* mouse retina are associated with deformations in the borders of the inner plexiform layer, and the *nr* Purkinje cell degeneration model eventually progresses to severe remodeling with time.

Cone loss in most retinal degenerations appears to activate formation of glial columns and seals, cell migration, neuronal loss, and rewiring. This large-scale glial remodeling is similar to that triggered in retinal detachment, including the migration of glial somata to the distal margin (Lewis et al., 2002). The repositioning of neurons is dramatic, and the presence of entire columns of neurons spanning the inner plexiform layer suggests that a nonselective migratory process is triggered. We have observed few instances of ganglion cell eversion to the inner nuclear layer, but this rarity is complicated by sampling, as inner nuclear layer inversion is roughly five times more probable just because of the number of cells involved. On balance, it appears that all cells can migrate once hypertrophied glial tracts have developed.

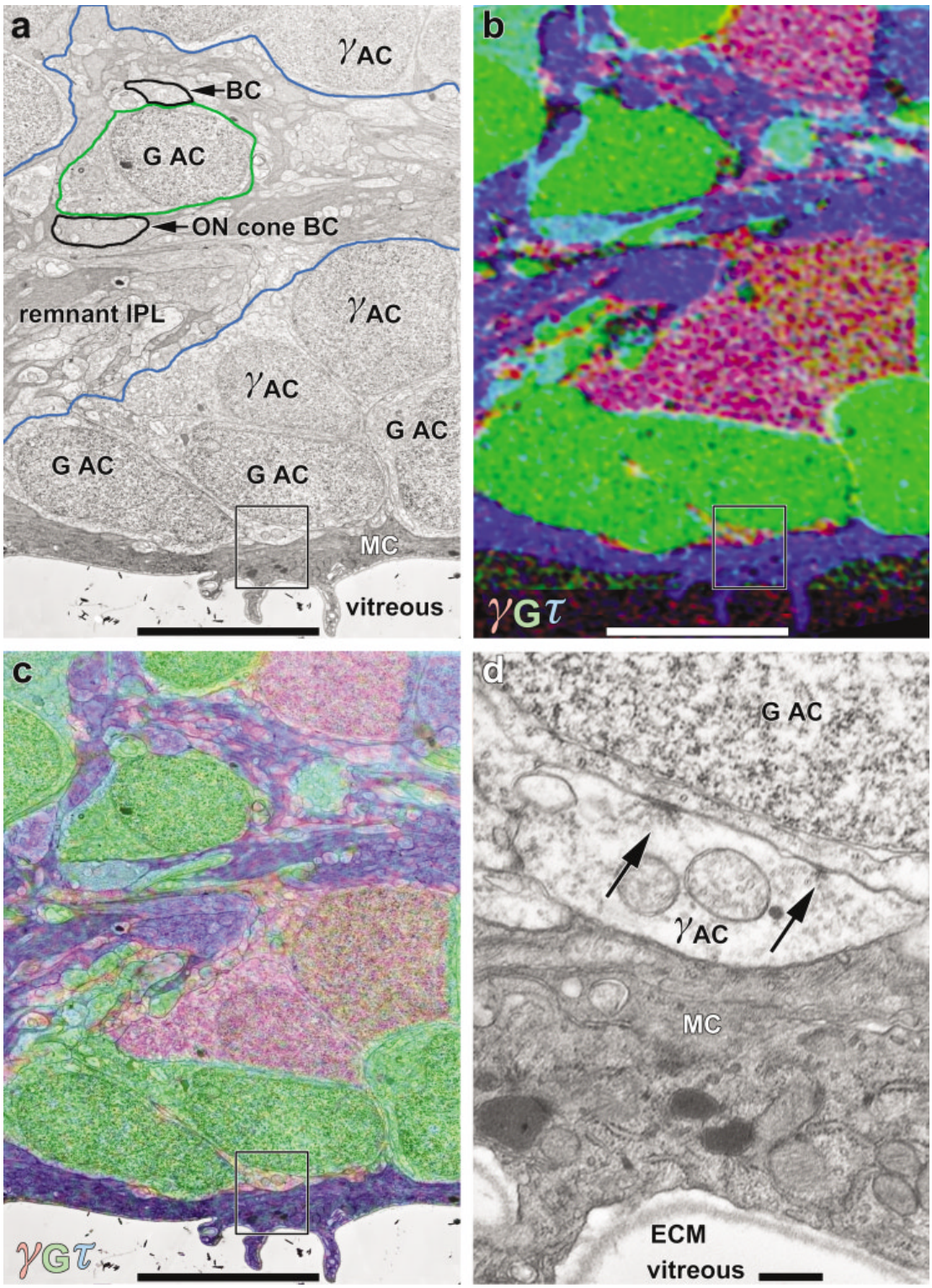

Fig. 6. Repositioned glycine+ and GABA+ amacrine cells in the former ganglion cell layer. **A:** Monochrome digital montage of glycine+ and GABA+ amacrine cells after migration into the ganglion cell layer, bordered proximally by Müller cell processes and the vitreous and distally by a strip of remnant inner plexiform layer, outlined in blue. A single glycine+ amacrine cell (outlined in green) within the remnant inner plexiform layer is completely surrounded by neuropil. **B:** Registered γGτ → rgb mapping of the same field. **C:** Overlay of the γGτ image on the ultrastructural channel. **D:** Enlarged inset (box) of two GABA+ amacrine cell presynaptic sites (arrows) on the soma of a repositioned glycine+ amacrine cell. Abbreviations as in Figure 2. ECM, extracellular matrix. Scales bars = 10 μm in A–C; 500 nm in D.

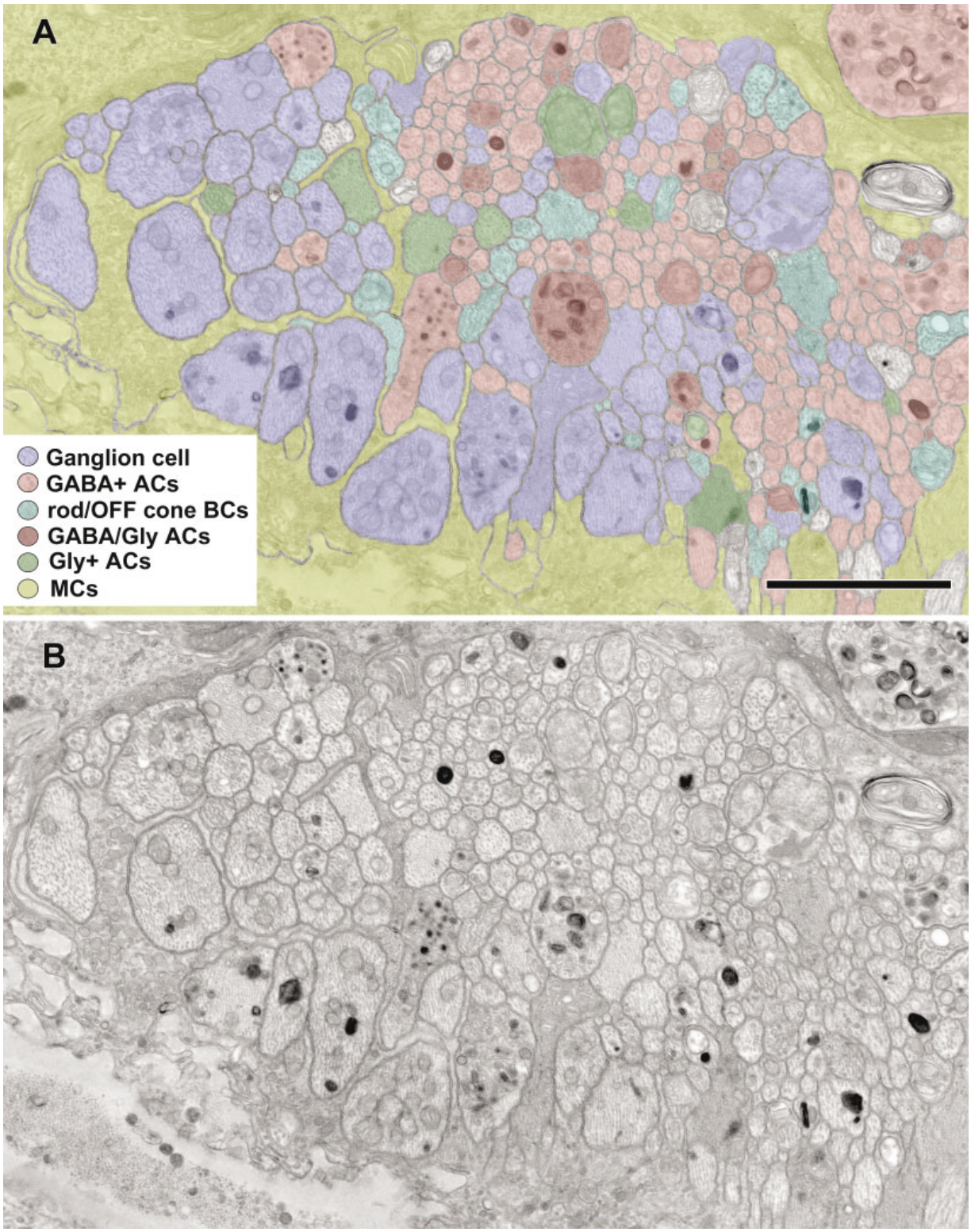

Fig. 7. Neurite fascicle ≈ 2 μm away from the distal margin of the retina and the Müller cell seal. **A:** Ultrastructural theme map. Six classes of elements are color-coded according to characteristic signatures: ganglion cells (blue; high glutamate, low taurine); GABAergic amacrine cells (light red; high GABA), glycinergic amacrine cells (olive; high glycine), a mixed glycine+ and GABA+ class (dark red); bipolar cells (cyan, high glutamate, high taurine); Müller cells (yellow, high taurine, high glutamine). Unclassified elements are not colored. **B:** The corresponding monochrome ultrastructural channel. Scale bar = 250 nm in A.

We cannot discount the effects of glial hypertrophy in reshaping the retina, but this hypothesis does not easily account for phenomena such as bidirectional displacement of cells. We believe that these data, although composed of static images, do reflect dynamic activity and cellular migration similar to a developmental time series. For instance, relocated amacrine cells from the inner nuclear layer have distinctive signatures and are not present in the ganglion cell layer of younger animals within models that, at later time points, exhibit bona fide glycinergic amacrine cells in the ganglion cell layer, leading us to conclude that these cells are either migrating (Sullivan et al., 2003) or are being forced by glial elements into the ganglion cell layer. Conversely, other neuronal classes do not migrate, but are in abnormal locations due to massive loss of photoreceptor and bipolar cell populations.

We have not used cell counts to document cell death for three reasons. First, many retinal degeneration models display obvious depletion of the ganglion cell and inner nuclear layers, with regions devoid of ganglion or amacrine cell and bipolar cells (Fig. 4D) or with reduction of the inner nuclear layer to a thickness of only two cells at certain points (Fig 4C). Second, nearly all the samples we have employed were archival, osmicated resin-embedded tissues acquired over a span of 30 years and could not be used for conventional whole mount methods. Third, cell loss is clearly focal in many cases, and patches of depleted retina are adjacent to those containing nearly normal numbers (Fig. 4B). Global cell counts would not capture this spatial inhomogeneity. We have not observed compensatory thickening of any cell layers that would reasonably account for depletion in others. It is also unlikely that neurons could be caught in apoptotic states (if generic apoptosis is the mechanism) during remodeling. If the inner nuclear layer is reduced in thickness by 50% over a period of 150 days, a uniform rate of cell death would mean that only 3 in 1,000 cells would actually be in the process of dying at any sample point. This number would be smaller for slower remodeling systems and undetectable in most cell death visualization protocols.

Rewiring accompanying new neurite extension, microneuroma formation, evolution of new synaptic contacts in the ganglion cell and remnant inner nuclear layers, loss of retinal neurons, and globally disturbed retinal topology implies that remodeled retinas are unlikely to process visual signals properly. Furthermore, if the apparent bipolar → bipolar cell contacts we have observed are functional, they represent re-entrant circuits that can display resonance and instability, providing network-driven excitation in the absence of photoreceptor inputs. The triggers for this profusion of new synapses and the mechanisms by which partners are found are clearly important issues. However, remodeling appears to be a classical CNS deafferentation response in many respects, and we expect that similar molecular mechanisms are probably involved. Physical or environmental deafferentation of sensory pathways evokes atrophy of targeted neurons (Von Noorden and Crawford, 1978; Levitt et al., 2001) and remodeling in corticothalamic circuits in adult mammals (Buonomano and Merzenich, 1998; Jones and Pons, 1998). Degeneration of the sensory retina clearly triggers similar effects in the surviving neural retina. Defects in cone-driven OFF channel circuits occur long before photoreceptor degeneration is complete in transgenic pigs with rhodopsin gene defects (Banin et al., 1999), suggesting that subtle rewiring (Peng et al., 2000) may be a persistent process that erupts into full-scale late remodeling upon loss of all afferent signaling. We hypothesize that global neural remodeling in degenerating retinas is, in part, an active process that restores essential trophic signals to neurons, perhaps through re-entrant signals that set up oscillatory excitations. Indeed, RP patients often report photopsias (scintillating photic illusions) consistent with erratic, nonspecific signaling in the surviving neural retina (Weleber and Gregory-Evans, 2001). More importantly, recent physiological data suggest that retinal connectivity, or at least synaptic efficacy, is shaped by postnatal visual experience (Tian and Copenhagen, 2001), and, considering the extent of plasticity in adult neural retinas long after the degeneration of the sensory retina, it is plausible to hypothesize incipient plasticity as an attribute of the normal adult retina.

Retinal rescue strategies will have to confront remodeling and circuit corruption in addition to overcoming simple neuronal loss. The distal glial seal must be breached to add new progenitor/stem cells, and, even then, cell-based therapies may not reverse degeneration, as new cells may be co-opted to produce aberrant wiring by the remodeling retina (Li et al., 1995). The possibility of stem cell fusion (Terada et al., 2002) with host neurons is also a serious impediment to rescue and analysis. There is as yet no evidence that transplantation can stop or delay remodeling, and the possibility of transplanting cells into the retina without triggering further remodeling seems doubtful. Bionic implants are similarly impacted. The subretinal chip strategy also requires traumatic breach of the glial seal and depends on normal retinal topology (Zrenner et al., 1998; Zrenner, 2002), which remodeling abrogates. Epiretinal implants are compromised by rewiring, probable re-entrant excitation of the retina through ganglion cell-amacrine cell coupling (Xin and Bloomfield, 1997; Marc and Jones, 2002), ganglion cell death, and migration-induced disorder in the ganglion cell layer.

The initiators of remodeling are unknown and may constrain therapeutic windows for genetic and molecular rescues, such as survival factor delivery (Faktorovich et al., 1990). If rescues are to proceed, prevention of remodeling may have to precede intervention. On the other hand, the exuberance of synaptic remodeling is provocative, for if neurons in the retina can make novel synapses and circuits, might they not be retrained with patterned competitive inputs?

ACKNOWLEDGMENTS

The authors thank Maggie Shaw and Jia-Hui Yang for technical assistance.

LITERATURE CITED

Banin E, Cideciyan AV, Alemán TS, Petters RM, Wong F, Milam AH, Jacobson SG. 1999. Retinal rod photoreceptor-specific gene mutation perturbs cone pathway development. Neuron 23:549–557.

Blanks JC, Mullen RJ, LaVail MM. 1982. Retinal degeneration in the pcd cerebellar mutant mouse. II. Electron microscopic analysis. J Comp Neurol 212:231-246.

Buonomano DV, Merzenich MM. 1998. Cortical plasticity: from synapses to maps. Annu Rev Neurosci 21:149–186.

Burmeister M, Novak J, Liang MY, Basu S, Ploder L, Hawes NL, Vidgen D, Hoover F, Goldman D, Kalnins VI, T.H. R, Taylor BA, Hankin MH, McInnes RR. 1996. Ocular retardation mouse caused by Chx10 homeobox null allele: impaired retinal progenitor proliferation and bipolar cell differentiation. Nat Genet 12:376–384.

Campbell DB, Hess EJ. 1996. Chromosomal localization of the neurological mouse mutations tottering (tg), Purkinje cell degeneration (pcd), and nervous (nr). Mol Brain Res 37:79–84.

Chen J, Woodford B, Jiang H, Nakayama T, Simon M. 1993. Expression of a C-terminal truncated rhodopsin gene leads to retinal degeneration in transgenic mice. Invest Ophthalmol Vis Sci 34:S333.

Chow AY, Chow VY. 1997. Subretinal electrical stimulation of the rabbit retina. Neurosci Lett 225:13–16.

Coffey PJ, Girman S, Wang SM, Hetherington L, Keegan DJ, Adamson P, Greenwood J, Lund RD. 2002. Long-term preservation of cortically dependent visual function in RCS rats by transplantation. Nat Neurosci 5:53–56.

D' Cruz PM, Yasumura D, Weir J, Matthes MT, Abderrahim H, LaVail MM, Vollrath D. 2000. Mutation of the receptor tyrosine kinase gene Mertk in the retinal dystrophic RCS rat. Hum Mol Genet 9s:645–651.

de Raad S, Szczesny PJ, Munz K, Reme CE. 1996. Light damage in the rat retina: glial fibrillary acidic protein accumulates in Müller cells in correlation with photoreceptor damage. Ophthalmic Res 28:99–107.

Faktorovich EG, Steinberg RH, Yasumura D, Matthes MT, LaVail MM. 1990. Photoreceptor degeneration in inherited retinal dystrophy delayed by basic fibroblast growth factor. Nature 347:83–86.

Fariss RN, Li Z-Y, Milam AH. 2000. Abnormalities in rod photoreceptors, amacrine cells, and horizontal cells in human retinas with retinitis pigmentosa. Am J Ophthalmol 129:215–223.

Fei Y. 2002. Cone neurite sprouting: an early onset abnormality of the cone photoreceptors in the retinal degeneration mouse. Mol Vis 8:306–314.

Fernandez-Gonzalez A, La Spada AR, Treadaway J, Higdon JC, Harris BS, Sidman RL, Morgan JI, Zuo J. 2002. Purkinje cell degeneration (pcd) phenotypes caused by mutations in the axotomy-induced gene, Nna1. Science 295:1904–1906.

Fintz AC, Audo I, Hicks D, Mohand-Said S, Leveillard T, Sahel J. 2003. Partial characterization of retina-derived cone neuroprotection in two culture models of photoreceptor degeneration. Invest Ophthalmol Vis Sci 44:818–825.

Fletcher EL, Kalloniatis M. 1996. Neurochemical architecture of the normal and degenerating rat retina. J Comp Neurol 376:343–360.

Frederick JM, Krasnoperova NV, Hoffmann K, Church-Kopish J, Rüther K, Howes K, Lem J, Baehr W. 2001. Mutant rhodopsin transgene expression on a null background. Invest Ophthalmol Vis Sci 42:826–833.

Green ES, Stubbs JL, Levine EM. 2003. Genetic rescue of cell number in a mouse model of microphthalmia: interactions between Chx10 and G1-phase cell cycle regulators. Development 130:539–552.

Humayun MS, de Juane EJ, Dagnelie G, Greenberg RJ, Propst RH, Phillips DH. 1996. Visual perception elicited by electrical stimulation of retina in blind humans. Arch Ophthalmol 114:40–46.

Humayun MS, Prince M, de Juan EJ, Barron Y, Moskowitz M, Klock IB, Milam AH. 1999. Morphometric analysis of the extramacular retina from postmortem eyes with retinitis pigmentosa. Invest Ophthalmol Vis Sci 40:143–148.

Humphries MM, Rancourt D, Farrar GJ, Kenna P, Hazel M, Bush RA, Sieving PA, Sheils DM, McNally N, Creighton P, Erven A, Boros A, Gulya K, Capecchi MR, Humphries P. 1997. Retinopathy induced in mice by targeted disruption of the rhodopsin gene. Nat Genet 15:216–219.

Jones BW, Baehr W, Frederick JM, Marc RE. 1999. Aberrant remodeling of the neural retina in the GHL transgenic mouse. ARVO.

Jones EG, Pons TP. 1998. Thalamic and brainstem contributions to large-scale plasticity of primate somatosensory cortex. Science 282:1121–1125.

Kalloniatis M, Marc RE, Murry RF. 1996. Amino acid signatures in the primate retina. J Neurosci 16:6807–6829.

Keeler C. 1966. Retinal degeneration in the mouse is rodless retina. J Hered 57:47–50.

Landis SC. 1975. Histochemical demonstration of mitochondrial dehydrogenases in developing normal and nervous mutant mouse Purkinje cells. J Histochem Cytochem 23:136–143.

LaVail MM, Sidman RL, Gerhardt CO. 1975. Congenic strains of RCS rats with inherited retinal dystrophy. J Hered 66:242–244.

LaVail MM, Blanks JC, Mullen RJ. 1982. Retinal degeneration in the pcd cerebellar mutant mouse. I. Light microscopic and autoradiographic analysis. J Comp Neurol 212:217–230.

LaVail MM, White MP, Gorrin GM, Yasumura D, Porrello KV, Mullen RJ. 1993. Retinal degeneration in the nervous mutant mouse. I. Light microscopic cytopathology and changes in the interphotoreceptor matrix. J Comp Neurol 333:168–181.

Levitt JB, Schumer RA, Sherman SM, Spear PD, Movshon JA. 2001. Visual response properties of neurons in the LGN of normally reared and visually deprived macaque monkeys. J Neurophysiol 85:2111–2129.

Lewis GP, Charteris DG, Sethi CS, Fisher SK. 2002. Animal models of retinal detachment and reattachment: identifying cellular events that may affect visual recovery. Eye 16:375–387.

Li ZY, Kljavin IJ, Milam AH. 1995. Rod photoreceptor neurite sprouting in retinitis pigmentosa. J Neurosci 15:5429–5438.

Liu IS, Chen JD, Ploder L, Vidgen D, van der Kooy D, Kalnins VI, McInnes RR. 1994. Developmental expression of a novel murine homeobox gene (Chx10): evidence for roles in determination of the neuroretina and inner nuclear layer. Neuron 13:377–393.

Machida S, Kondo M, Jamison JA, Khan NW, Kononen LT, Sugawara T, Bush RA, Sieving PA. 2000. P23H rhodopsin transgenic rat: correlation of retinal function with histopathology. Invest Ophthalmol Vis Sci 41:3200–3208.

Marc RE. 1999. Mapping glutamatergic drive in the vertebrate retina with a channel-permeant organic cation. J Comp Neurol 407:47–64.

Marc RE, Cameron DA. 2002. A molecular phenotype atlas of the zebrafish retina. J Neurocytol 30:593–654.

Marc RE, Jones BW. 2002. Molecular phenotyping of retinal ganglion cells. J Neurosci 22:412–427.

Marc RE, Liu W. 2000. Fundamental GABAergic amacrine cell circuitries in the retina: nested feedback, concatenated inhibition, and axosomatic synapses. J Comp Neurol 425:560–582.

Marc RE, Murry RF, Basinger SF. 1995. Pattern recognition of amino acid signatures in retinal neurons. J Neurosci 15:5106–5129.

Marc RE, Murry RF, Fisher SK, Linberg KA, Lewis GP, Kalloniatis M. 1998. Amino acid signatures in the normal cat retina. Invest Ophthalmol Vis Sci 39:1685–1693.

Marc RE, Jones BW, Yang JH, Shaw MV, Milam AH. 2001. Molecular phenotyping of the neural retina in retinitis pigmentosa. Invest Ophthalmol Vis Sci 42:S117.

Masland RH. 2001. Neuronal diversity in the retina. Curr Opin Neurobiol 11:431–436.

Mohand-Said S, Deudon-Combe A, Hicks D, Simonutti M, Forster V, Fintz A-C, Léveillard T, Dreyfus H, Sahel J-A. 1998. Normal retina releases a diffusible factor stimulating cone survival in the retinal degeneration mouse. Proc Natl Acad Sci U S A 95:8357–8362.

Mullen RJ, LaVail MM. 1975. Two types of retinal degeneration in cerebellar mutant mice. Nature 258:528–530.

Peng YW, Hao Y, Petters RM, Wong F. 2000. Ectopic synaptogenesis in the mammalian retina caused by rod photoreceptor-specific mutations. Nat Neurosci 3:1121–1127.

Pittler SJ, Keeler CE, Sidman RL, Baehr W. 1993. PCR analysis of DNA from 70-year-old sections of rodless retina demonstrates identity with the mouse rd defect. Proc Natl Acad Sci U S A 90:9616–9619.

Robb RM, Silver J, Sullivan RT. 1978. Ocular retardation (or) in the mouse. Invest Ophthalmol Vis Sci 17:468–473.

Santos A, Humayun MS, de Juan EJ, Greenburg RJ, Marsh MJ, Klock IB, Milam AH. 1997. Preservation of the inner retina in retinitis pigmentosa. A morphometric analysis. Arch Ophthalmol 115:511–515.

Scarlatis G. 2000. Optical prosthesis: visions of the future. JAMA 283: 2297.

Steinberg R, Flannery J, Naash M, Oh P, Matthes M, Yasumura D, Lau-Villacorta C, Chen J, LaVail M. 1996. Transgenic rat models of inherited retinal degeneration caused by mutant opsin genes. Invest Ophthalmol Vis Sci 37:5698.

Stone JL, Barlow WE, Humayun MS, de Juan EJ, Milam AH. 1992. Morphometric analysis of macular photoreceptors and ganglion cells in retinas with retinitis pigmentosa. Arch Ophthalmol 110:1634–1639.

Strettoi E, Pignatelli V. 2000. Modifications of retinal neurons in a mouse model of retinitis pigmentosa. Proc Natl Acad Sci U S A 97:11020–11025.

Strettoi E, Porciatti V, Falsini B, Pignatelli V, Rossi C. 2002. Morphological and functional abnormalities in the inner retina of the rd/rd mouse. J Neurosci 22:5492–5504.

Strettoi E, Pignatelli V, Rossi C, Porciatti V, Falsini B. 2003. Remodeling of second-order neurons in the retina of rd/rd mutant mice. Vision Res 43:867–877.

Sullivan R, Penfold P, Pow DV. 2003. Neuronal migration and glial remod-

eling in degenerating retinas of aged rats and in nonneovascular AMD. Invest Ophthalmol Vis Sci 44:856–865.

Terada N, Hamazaki T, Oka M, Hoki M, Mastalerz DM, Nakano Y, Meyer EM, Morel L, Petersen BE, Scott EW. 2002. Bone marrow cells adopt the phenotype of other cells by spontaneous cell fusion. Nature 16:542–545.

Tian N, Copenhagen DR. 2001. Visual deprivation alters development of synaptic function in inner retina after eye opening. Neuron 32:439–449.

van Nie R, Ivanyi D, Demant P. 1978. A new H-2-linked mutation, rds, causing retinal degeneration in the mouse. Tissue Antigens 12:106–108.

Villegas-Perez MP, Lawrence JM, Vidal-Sanz M, Lavail MM, Lund RD. 1998. Ganglion cell loss in RCS rat retina: a result of compression of axons by contracting intraretinal vessels linked to the pigment epithelium. J Comp Neurol 392:58–77.

Von Noorden GK, Crawford MLJ. 1978. Morphological and physiological changes in the monkey visual system after short-term lid suture. Invest Ophthalmol Vis Sci 17:762–768.

Weleber R, Gregory-Evans K. 2001. Retinitis pigmentosa and allied disorders. In: Ogden TE, Hinton DR, editors. Retina: basic science, inherited disease and tumors. St Louis: Mosby. p 362–460.

Xin D, Bloomfield SA. 1997. Tracer coupling pattern of amacrine and ganglion cells in the rabbit retina. J Comp Neurol 383:512–528.

Young MJ, Ray J, Whiteley SJO, Klassen H, Gage FH. 2000. Neuronal differentiation and morphological integration of hippocampal progenitor cells transplanted to the retina of immature and mature dystrophic rats. Mol Cell Neurosci 16:197–205.

Zrenner E. 2002. Will retinal implants restore vision? Science 295:1022–1025.

Zrenner E, Gabel VP, Haemmerie H, Hoefflinger B, Shubert M. 1998. Subretinal implants. Ophthalmic Res 30:197–198.